November 1986 LRP 307/86

FUNDAMENTAL PLASMA PHENOMENA

R.A. Stern

Invited Lectures presented at

the Course and Workshop on

Basic and Advanced Fusion Plasmas Diagnostic Techniques

Villa Monastero - Varenna - Italy

September 3 - 13, 1986

EUR 10797-EN

FUNDAMENTAL PLASMA PHENOMENA

R.A. STERN *

Centre de Recherches en Physique des Plasmas
Association Euratom - Confédération Suisse
Ecole Polytechnique Fédérale de Lausanne
21, Av. des Bains, CH-1007 Lausanne / Switzerland

ABSTRACT

The relationship between theory, measurement methods and experiment in basic plasma research is discussed. Illustrations are given from recent studies which use and develop new techniques for characterizing complex phenomena, such as static and dynamic field-particle interactions and transport. The status, limitations and possibilities of selected diagnostics are presented.

I. INTRODUCTION

The experimental study of basic processes in plasmas is closely linked to progress in diagnostic methods, and has been a source of measurement techniques useful also in fusion and applied plasma areas. Basic plasma physics has adapted and drawn from all fields, most recently atomic physics and laser technologies. The rapid advances of these disciplines make it very likely that new and powerful plasma methods will continue to emerge through their use. This requires familiarity with their principles and attention to developments, in fact an effort comparable to that expended on plasma physics itself.

* Visiting Professor. Permanent address: University of Colorado, Boulder, U.S.A.

Work supported by the Swiss National Science Foundation (Grants No. 2.868.085 and 2.869.085) and by the US National Science Foundation (Grants INT-8405076 and PHY-8312489).

Our lectures present selected concepts underlying modern diagnostics derived from atomic and laser physics and used to probe the fundamental properties of plasmas.

i. For illustrations we choose, from recent experiments, that sub-set which has most needed and developed observation techniques [1]. These turn out to be experiments concerned with some processes of highest complexity: the space - and time evolution of plasma in electric and magnetic fields intense enough to cause strong field - particle interactions, e.g. secular modifications of the Boltzmann velocity distribution function.

ii. The presentation is organized to reflect the hierarchy of factors guiding a typical experimental program. The starting point for diagnostics is normally the description of the physical quantities involved, as determined by the theoretical approach and its level. This is illustrated here in Section II. Representation, which demonstrates the use of both the kinetic and fluid formalisms in approaching the field-particle problem. The next stage, in response to the requirements imposed by the description, is the development of an appropriate measurement scheme. For particle interactions involving ions, this turns out to be Laser-Induced Fluorescence (LIF), recent (and in part unpublished) versions of which are presented in Section III. In sequence, the synthesis of representation and measurement can lead to new findings which call for, and generate advanced techniques, as illustrated in IV. Irreversible processes, which are concerned with causality and transport. The closing section V. Time, Space and Quantum Effects, points out some complexities and limits inherent in the new diagnostics.

II. REPRESENTATION

The diagnostic task is the description of plasma properties at the highest level, as required by the physics of the process. The most demanding problem arises in current studies of wave - and field -particle interactions. These have reached the stage where the kinetic represen-

tation with full phase-space detail must be tackled. In principle, this means that the one-particle distribution function f(v ; x , t) for all species (electrons and ions) should be measured, as well as the fields E(x , t) and B(x , t). Further, some measure of causality is needed, i.e. a tracing of particles along trajectories in phase space. Modern diagnostic methods are being developed which begin to meet these requirements, and will be described below. We note for the future that even more complicated descriptions are needed to solve problems posed by forefront theoretical work, e.g. correlations and similar concepts which go beyond the one-particle distribution function representation.

Note that the fields E, B are functions of the space and time coordinates only, whereas the distribution function contains the "microscopic" velocity v, which functions mathematically as a dummy variable when integrating moments of f to calculate fluid ("macroscopic") quantities such as density, flow velocity and temperature. Integrals of kinetic equations (e.g. the Boltzmann equation) which destroy f, leave E and B in the picture, linked to the macroscopic quantities, which are evidently much easier to measure than f itself. This means that the data interpretation may be performed in two stages: the simpler fluid description can be used to measure densities and velocities which are consistent with and yield the field values without requiring a direct measurement.

A. The Kinetic Representation

As an illustration we consider an adaptation of a current theoretical problem in the strong interaction between fields and particle distribution functions, in which perturbation approaches are inadequate. Instead, the Boltzmann equation must be fully solved. These studies were originally motivated by questions in gas-discharge physics [2], but have evident extensions to other areas. Such situations arise whenever the plasma supports (i.e. can only partially shield itself from) electric and magnetic fields, and these are so strong that the plasma thermodynamic description lies far from the locus of equilibrium states. Then properties such as temperature, pressure, density and fluid velocity and the relationships between them must be reviewed, and

may not be realistic. Instead one uses - at the lowest level - the single-particle distribution function f, which connects to the thermodynamic properties by means of moment integrals. In this formulation field-induced changes in f are evaluated, and automatically and simultaneously yield the corresponding changes in T, p, n, V, without postulating a relationship betweem them. Most important, irreversible processes such as collisions can be incorporated into the physics at this stage, without recourse to phenomenological coefficient.

The case we analyze is the plasma state in uniform, stationary electric and magnetic fields, which "distort" f away from the field-free Maxwellian form, while their effect is balanced by particle collisions which tend to randomize the velocity distribution. Then f is governed by the Boltzmann equation, which has the form (in the steady-state, spatially homogenous limit):

$$F \cdot \frac{df}{dv} = n \iint\!\!\ldots\!\int \left[f'g' - fg \right] \sigma \, |v - v_a| \, d^3 v_a \, d\Omega \qquad (1)$$

Here F represents the force term, = (e/m)(E + (v×B)/c) for a species with charge/mass ratio e/m. The RHS is the usual collision integral, representing encounters between species characterized by the distribution functions f(v) and $g(v_a)$. The primes refer to velocities after collision, σ is the cross-section, $|v-v_a|$ the relative velocity, and the integration is over the solid angle and the velocities of the "target" species a, whose density is n.

A case for which a simple closed-form solution can be obtained, and which is physically significant, is that of (head-on) charge exchange between ions and their parent-gas atoms [3]. This applies to noble-gas discharge plasmas, including devices used in experiments on basic phenomena. Here $g = n\delta(v_a)$ represents cold atoms, presumably in good thermal contact with the vessel wall, and a separate equation for g is not needed. Now the relative velocity → v. If the range of velocities v (the ion temperature) is limited, and the cross-section σ is

relatively insensitive, the integrations on the RHS can be performed and reduce to:

$$n\tilde{\sigma}\delta(v)\iint f(v)\,v\,d^3v - n\tilde{\sigma}vf(v) \tag{2}$$

Here σ incorporates the solid-angle integration and n is the atom (target) density. For convenience, define the y-coordinate to be parallel to the force F. Consider first the case when the dependence of F on v may be neglected. Then the formal solution to the Boltzmann equation is:

$$f \cong C\delta(v_z)\,\delta(v_x)\,S(v_y)\exp-\left[n\tilde{\sigma}\,v_y^2/2F\right] \tag{3}$$

where s is the Heaviside step-function. The distribution turns out to be a half-Maxwellian, with the coldest particles at v = 0 resulting from charge exchange of atoms into unaccelerated ions. Note, however, that the parameter describing the thermal width is $T^* = mF/n\tilde{\sigma}$, i.e., the field and the collisionality combined play the role of a temperature. It is easy to see that, since the $v\times B \cdot (df/dv)$ component of $F \cdot (df/dv) \to 0$ for this quadratic form, $T^* = eEL$, where $L^{-1} = n\tilde{\sigma}$ is the mean-free path for collisions. Here the pseudo-temperature is just the energy acquired by the particle of charge e under the influence of the electric field E while undergoing free drift in between collisions. That is, this process represents the conversion of directed field energy into random "kinetic" particle energy via charge-exchange collisions. This appears paradoxical, since charge-exchange collisions are obviously a source of energy loss: the answer is that the field constitutes a source of free energy, so that energy is indeed lost from the system, nevertheless the system is maintained in a non-equilibrium state of higher temperature by the process, than would be the case in the absence of the field.

B. The Fluid Description

Conceptually, a complete diagnostic solution of this problem requires the measurement of f, g, and F. If the experiment is carried out in a gas-discharge plasma, the initial, cold ion temperatures are of order 0.1 - 1 eV, and the mean-free paths must be smaller than machine size, say 1 to 100 cm. Hence the electric field strengths

which will make the pseudo-temperature equal to the background are of order 10 V/cm. This is far less than the detectable minimum using Stark effect, which is useful in fields comparable to the atomic binding fields, typically 10 kV/cm. An approach we can take is to fall back on the lower level of representation, the fluid conservation equations, equivalent to weighted integrations of the Boltzmann equation. The fluid momentum equation then has the form:

$$F = \frac{e}{m}\left[E + \frac{V \times B}{c}\right] = \nu V \tag{4}$$

where ν is a phenomenological collision frequency. Note that, consistent with the conditions we imposed on the Boltzmann equation, this is the steady-state and spatially homogeneous equation, so that the $V \cdot \nabla V$ and ∇p terms are neglected. Since in fact they can be measured (as shown below), corrections for these effects can be introduced and our conceptual result will be quite general.

We now restrict ourselves to a specific configuration, crossed electric and magnetic fields. Let E define the x axis and B the z coordinate. Then the vector momentum equation separates into the two scalar expressions:

$$\begin{aligned} F_x &= \frac{e}{m} E \frac{\nu^2}{\nu^2 + \omega_c^2} = \nu V_x \\ F_y &= \frac{e}{m} E \frac{\nu \omega_c}{\nu^2 + \omega_c^2} = \nu V_y \end{aligned} \tag{5}$$

The ratio ν/ω of collision to cyclotron frequencies can be varied experimentally by changing the atom pressure or the magnetic field strength. One can, therefore, go to the limit $\nu/\omega_c \ll 1$, which yields above : $V_y \cong cE/B$;

$$F_x \ll F_y = \frac{e}{m} E \frac{\nu}{\omega_c} \tag{6}$$

We have thus isolated one fluid macroscopic property which is directly related to the electric field strength E. In terms of sensitivity, note that the ratio cE/B has the value 10^5 cm/sec for E = 1 V/cm and B = 1kG. Thus an ion distribution function of less than 1 eV temperature, common in gas discharge plasmas, will allow a directed drift velocity caused by a 1 V/cm field to be detected in a 1 kG background magnetic field. In other words, the plasma fluid drift serves as a sen-

sitive diagnostic of the electric field. This will be illustrated at the end of the following section, in an experiment which shows the fluid drift $\propto E$, and the ion velocity distribution function depending on E, as expected.

Such a lower-level analysis also enables us to evaluate the form of the kinetic distribution function for this complex geometry. As eqs. (5) and (6) have shown, the main response of the plasma to the crossed-field configuration is a drift V_y, whose value is such that, in the absence of collisions, the Lorentz force would balance out the electric field, leaving a net zero force. The effect of weak collisions is to induce a small force, the dominant component being $F_y = \nu V_y$, consistent with the dominant drift and a finite collisional momentum loss rate ν. We now use this result as a Born-approximation for the force F in the kinetic analysis, above. In this limit the force depends principally on the mean speed, and only weakly on the range of kinetic velocities v. The use of the formal solution eq. (3) is then allowed, with substitution of $F \cong F_y = \nu V_y$, a constant. The pseudo-temperature $T^* \Rightarrow m\nu V_y/n\bar{\sigma}$. Further, since the mean-free path $L = (n\bar{\sigma})^{-1}$ can be approximated by the ratio V_y/ν (a definition of ν, in a sense) it follows that $T^* = mV_y^2$. This rough result is consistent with the fact that the E-field maintains the plasma drift energy at a fixed value despite equal-mass collisions, which tend to convert the drift (ordered) to disordered (thermal) energy.

C. Experimental Test

Putting together the results of the analysis, carried out at the two levels of representation used above, we are led to the following diagnostic task: a complete description of the field-particle interaction in the steady state requires a measurement of the kinetic velocity spread (the relative number of ions having a velocity component v_y in the direction normal to the electric and magnetic field), plus a measurement of the mean drift velocity V_y (used here as a lowest-order estimate of the electric field). This description is attainable using LIF, as discussed in detail below. Anticipating for the moment the discussion, typical results of such an experiment are illustrated

by the raw data (unreduced observations), shown in Fig. 1. The figure shows ion distribution functions measured in the absence of the electric field (the central, narrow resonance), as well as in the presence of the field. Note first that the field shifts the center of the distribution function in opposite directions, depending on the direction of the field. As will be shown below, the magnitude of the shift is proportional to the intensity of the field. Thirdly, the width of the resonance (pseudo-temperature) has increased considerably, but is roughly the same for the two distributions shifted in opposite directions: it turns out that it depends linearly on the intensity, not the direction of the field. That is, the physical dependences predicted by the analysis are verified, using this single technique.

What is more, the shape of the resonances at very strong fields, as in the figure, turn out to differ sensibly from the Maxwellian predicted above. When the experiment is performed in a geometry with strong spatial gradients and time evolution, additional physical features appear in the data which can be associated with processes not considered in the simple analysis. That is, the fine-scale diagnostic chosen yields more detail and information than required by the lowest-order representation, and guides us towards processes which come into play at higher intensities. It is tempting to define, therefore, an interesting diagnostic technique as one which not only answers the questions, but also poses new and presumably intelligent ones.

III. ION DISTRIBUTION FUNCTION MEASUREMENTS USING LASER-INDUCED FLUORESCENCE

As shown above, the representation compells the measurement of ionic drift and pseudo-temperature. A suitable diagnostic approach with widest applications and rapidly increasing use, is based on laser excitation of transitions between quantum states of particles in plasmas. This methodology has been used to measure quantities as diverse as atomic and ionic densities, velocities and temperatures, electron temperatures, as well as electric and magnetic fields in fusion and in basic research plasmas [4]. Since it derives from and closely follows

developments in laser spectroscopy - probably the most popular technique in atomic physics - LIF can be expected to provide continually new and improved resources for our use. That is, its potential for the future is very high.

A. Basic Concepts of Light/Atom Interaction

We sketch out here elementary deviation of rates and cross-sections involved in LIF. The common ground in LIF techniques involves an atomic or ionic species (test particle) which can exist in quantum states having discrete energies within the plasma, and a radiation source/laser generating photons with energy $h\nu$, which can be tuned over the energy range corresponding to the difference between some of the quantum states: $h\nu_n = E_{n+1} - E_n$. Under appropriate conditions, which we will seek to make strongly dependent upon the properties of the plasma, the radiation source beamed across the plasma will excite transitions between the states of the test particles. This manifests itself by one or more observable phenomena: enhanced absorption of the incident radiation, emission of radiation (fluorescence) at various wavelengths, ejection of particles (photoionization or detachment), and collisionality change (optogalavanic effect). The detection of these processes, and unfolding their relationship to the plasma properties. constitutes the diagnostic task. Figure 2 is a schematic of a typical geometry containing essential elements: laser, plasma and detection system.

In the symplest case, test particles in two possible quantum states E_1, E_2 with equal statistical weights are in stationary equilibrium with radiation characterized by the frequency ν and spectral energy density $\rho(\nu)$. Here the photon energy $h\nu$ matches the difference $E_2 - E_1$, and the transition between the states via absorption and emission of the photon is allowed by quantum rules. The radiation field resides in modes whose spectral density is given by the Rayleigh formula, $N(\nu) = 8\pi\nu^2/c^3$. Thus $\rho(\nu) = h\nu \cdot N \rightarrow 8\pi h\nu^3/c^3$. We use the Einstein coefficients A, B_{21} and B_{12} to describe the spontaneous decay and induced emission of state 2, and the induced absorption (excitation) of state 1 respectively. The Einstein conditions can be stated as follows:

$B_{21} = B_{12} \equiv B$ for detailed balance; and $A/B = N\,h\nu = 8\pi\,h\nu^3/c^3$ to represent the density of state ratios, i.e. the fact that spontaneous decay can take place in all modes of the radiation field, since the photon momentum can be conserved via particle recoil in any direction, while induced emission occurs into one mode only - that of the incident photon.

To compare this resonant photon-particle interaction with scattering, it is convenient to introduce the photon (number) intensity $I = \rho c/h\nu$, and the differential cross-section σ for induced emission, defined by $I\sigma d\nu = B\rho(\nu)$. Combining these with the preceding, one eliminates B and ρ to obtain:

$$\sigma = \frac{\lambda^2}{4} \cdot \frac{A}{2\pi d\nu} \qquad (7)$$

with the radiation wavelength $\lambda = c/\nu$. Obviously that part of the radiation spectrum which extends beyond the absorption bandwidth (a quantum concept, below) of the transition has no effect on the process, hence the effective spectral width of the radiation is limited to A, i.e. $A/d\nu = 2\pi$. The cross-section $\sigma = \lambda^2/4$ is therefore a very large quantity, typically 10^{-10} cm^2 in the visible ($\lambda = 5000$ A $= 5\times10^{-5}$ cm). Clearly low-power laser radiation can be used in LIF, well within the capabilities of commercial tunable lasers.

An estimate of the spectral width A^{-1} to which the laser radiation must be confined to be useful, may be obtained from dimensional considerations. The atom and its states are characterized by wave functions Ψ_1 and Ψ_2, the electron charge e, and its mean position given by the expectation value $\langle\Psi|r|\Psi_2\rangle$. The photon is described by its propagation vector k and the unit polarization vector $\hat{e}$. In order to match dimensions with the scalar A, these factors must combine in the proportion:

$$A = e^2\langle\psi^*|\hat{e}\cdot r|\psi\rangle^2 K^3/h$$

Since no direction of $\hat{e}$ relative to r is preferred, the product $\hat{e} \cdot r = r\sin\theta\cos\phi$, $\sin\phi$ (for the two polarizations of the field) must be integrated over all angles, yielding a numerical factor $8\pi/3$. The result can be combined with the ratio A/B given above, to yield the

well-known formulae:

$$A = \frac{4}{3}\,\mu^2 K^3/\hbar \;;\; B = \frac{8\pi^3}{3}\,\mu^2/h^2 \qquad (8)$$

where μ is the electric dipole matrix element of the transition. Note that, for typical particles, in the visible A corresponds to a bandwidth of order 10^8 Hz or less.

B. Atomic Physics

The underlying assumption is that laser-induced changes in the test particle quantum states have negligible or calculable effects on the plasma properties, so that the diagnostic is non-perturbing. Here one encounters a central problem which must be tackled when using LIF. It is due to the fact that the laser-induced changes are long-lived, so that the observable signal is generated, not by the original quantum state of the plasma, but rather by the multi-state, strongly perturbed system which results from the laser/test particle interaction. The connection between signal and the initial plasma state involves, for instance, excited states which are created in the plasma by the laser.

This, precisely, is the essential difference between LIF and scattering. The latter is an elastic process which starts and stops as soon as the radiation source has been turned on or off, i.e. has no characteristic times associated with it. Also, scattering leaves the target density and configuration unchanged. In contrast, LIF induces quasi-permanent changes in the quantum state populations, has turn-on times which depend on the intensity as well as the internal parameters (lifetimes) of the scatterer, and continues to generate radiation after the laser has stopped. Hence simple descriptions in terms of scattering cross-sections have only limited applicability. The basic equations for the use of LIF therefore require the solution of combined populations and radiation fields, to establish a reasonably direct relationship between signal and the "initial" plasma. We illustrate this process for a simple case: the 2-level quantum system.

The atomic physics is relatively straightforward. First, we con-

sider an isolated test particle initially at $t = t_o$ in the ground state G with wave function Ψ_G and energy E_G initially, possessing an excited state (Ψ_E, E_E), and a non-zero dipole matrix element $\mu \equiv \int d^3r \Psi_G^* r \Psi_E$ connecting the two states. A laser beam of intensity I, polarization (unit electric field vector) $\hat{e}$ and energy $h\nu \approx E_E - E_G$ incident on the test particles will induce transitions $G \rightarrow E$ at the rate g_G BI/c, where B is the induced absorption coefficient given by Eq. (8), and g_G is the statistical weight. The excited state E, on the other hand, becomes de-excited at the rate $[g_E BI/c + A]$, where A is the spontaneous decay rate given in frequency units by $32\pi^3\nu^3\mu^2/3hc^3$. The de-excitation occurs with emission of radiation, in part along the direction of the incident laser beam, and the remaining isotropically distributed in all directions. The latter is of principal diagnostic interest, because it can be differentiated in direction and often in wavelength from the incident laser beam, and so can be analyzed with highest signal/noise. The diagnostic is therefore the intensity I_f due to spontaneous decay of the E-state with rate A. Consequently it depends directly on the number of E-state particles created in the plasma by the incident beam, $I_f \propto AN_E$.

C. Evolution of State Densities

The exact time-evolution of state densities in a 2-level system coupled by resonant radiation is a central topic in atomic physics. In general, depending on parameters such as the product of field strength and dipole moment (the Rabi frequency), the evolution is non-monotonic and can even have oscillatory features [5].

Under simple conditions, e.g. at low field strengths the quantum-state densities N are adequately represented by the much simpler rate equation model of the type:

$$\frac{d}{dt} N_E = -AN_E - g_E \sigma I N_E + g_G \sigma I N_G \qquad (9)$$

In the most elementary case, test particles are entirely confined within the laser beam, i.e. no spatial variation is allowed. The terms on the RHS represent spontaneous and induced decay of the excited state, and induced excitation from the ground state, respectively. No

inhomogeneous (e.g. collisional) processes are considered at this stage.

For a 2-level system, the excited state decays only to the ground state. Equation (9) is then supplemented by the condition:

$$N_E + N_G = N_G(t = t_0) \tag{10}$$

The solution to this system is

$$N_E = N_G \frac{g_G \sigma I}{\Sigma g \sigma I + A} \left\{ 1 - \exp - \left[(\Sigma g \sigma I + A)(t - t_0) \right] \right\} \tag{11}$$

That is, the excited state population builds up linearly as $N_E(t) = N_g(t_o)\ g_G BI(t-t_o)$ at first, and eventually reaches the asymptote:

$$N_E \longrightarrow N_G(t_0) \frac{g_G \sigma I}{\Sigma g \sigma I + A} \tag{12}$$

What these equations show is that, despite the fact that the excited state E serves as an intermediate step, N_E and hence the detected signal I_f bear a direct relationship to the plasma ground state density $N_G(t_o)$. This is the desired diagnostic: even in such a simple case, however, some complicating factors enter. First, as indicated in eq. (11), the time dependence of N_E is only partially determined by that of N_G. Second, eq. (12) shows that, even after the intrinsic process due to the population changes has become stationary, the laser intensity I enters into the relationship. This warns us that in more realistic situations, e.g. 3-level systems, data unfolding may be less direct. Finally it is important to realize that even in pure 2-level systems - which are not always available - the ground state does not necessarily have an effective infinite lifetime. Typically one finds that the residence time of the ground-state particle within the finite-diameter laser beam is limited by its thermal or flow velocity, and may become comparable to the intrinsic time-dependences of the population changes. These effects, which basically affect data interpretation in LIF, are discussed below and in Section V.

D. Data Analysis

i. From Eq. (11), it is seen that I_f has an intrinsic time-dependence represented by the term in {..}, in addition to the variation with time t_o of the ground-state density $N_G(t_o)$. This time-dependence must be normalized out of $I_f(t)$ to yield $N_G(t_o)$; or else the technique becomes limited to measuring time-variations in N_G over scales slow in comparison with the e-folding time $[(g_g+g_E)I+A]^{-1}$ of the E-state population. The latter is acceptable since it is advantageous in many cases to work with systems with large A, which yield copious fluorescence and also lose their intrinsic time-dependence fast. Typically, for ions A can be 0 (10^8 sec^{-1}), and the laser intensity I such that the induced rate $g\sigma I$ is comparable to A. Hence the intrinsic e-folding time is of order 10 nsec, sufficiently short to allow diagnosis of changes in the (heavy) ion densities, temperatures, etc. Note also that at high laser intensities, N_E and I_f can become independent of I. Saturation of this type is, again, quite unlike the usual scattering processes, and can be taken advantage of since it ensures that fluctuations in I do not affect I_f, which now reflects the time-evolution of $N_G(t_o)$ solely. Similarily, focusing the radiation beam down to its limiting size, in principle a few wavelengths, one can usually restrict I_f to a laser volume which represents the spatial resolution. Scanning the laser beam in space therefore yields a dependence $I_f(x)$ which mirrors that of N_G. That is, the space and time-variation in N_G can be followed.

ii. The line-shape of the fluorescence I_f contains important information about the plasma and the fields. The fine details of $I_f(\nu_f)$, in the presence of strong laser excitation, are an important topic of current study in atomic physics. From the viewpoint of plasma diagnostics, however, the fine spectrum is over-shadowed by broader effects: Doppler broadening, Stark and Zeeman shifts [6].

To justify such simplifications, consider the case when I is weak, so that the excited state can be viewed as existing in the absence of intense radiation. i.e. a population of density N_E is maintained, on the average, by laser excitation from the ground state. These discrete

particles have a random lifetime $\tau = 1/A$, connected with emission of a photon with a center frequency ν. Spectral analysis of the photon corresponds to Fourier transform of the time-variation $e^{i\nu_f t} e^{-At}$, yielding a Lorentzian form $A/(\nu_f^2 + A^2)$. Sub-dividing the E-state population into groups with various velocities, the Doppler effect causes particles with v to emit at a shifted frequency $\nu_f + \Delta\nu = \nu_f(1 - (k\cdot v)/kc)$, where k is the propagation vector of the emitted radiation. Hence the line-shape $I_f(\nu_f) \propto A^2/[\nu_f^2(1 - (k\cdot v)/kc)^2 + A^2]$ describes the sub-population of E-state particles having a velocity $(k\cdot v)/k$ along the direction in which I_f is observed. To connect this measurement back with the plasma ground-state, note that the change in velocity between E and G states due to absorption of photon momentum and the recoil of E caused by emission, are small due to the large ion/atom mass. Thus $I_f(\nu_f)$ can provide a direct measure of the ground-state particle velocity distribution function.

iii. As an alternative to measuring the line-shape of I_f, one can use a narrow-band excitation laser with intensity $I(\nu)$ and tune ν across the absorption width of the test particles. Here again, one should in principle study the system consisting of ground and excited states co-existing with incident and emitted radiation. At relatively low intensities, however, this is not necessary, and it suffices to consider transition G → E to have the Lorentzian width dictated by the excited-state spontaneous decay rate A. Note that if G were not a true ground-state, the Wigner-Weisskopf formula connecting the width to the geometric mean of the two lifetimes would be used. Since the G-state consists of sub-groups with velocities v, the cross-section for excitation now becomes a function of frequency and velocity with a form such as:

$$\sigma = \sigma_0 \frac{(A/2)^2}{[\nu - \nu_f(1 - K\cdot V/KC)]^2 + (A/2)^2} \qquad (13)$$

where k now is the propagation vector of the incident laser beam. That is, the excited-state population is selectively enhanced in velocity space. The evolution of $N_E(t,v)$ is given, for a 2-level system, by Eq. (11) with substitution of Eq. 13 for σ, in terms of $N_G(t_o,v)$. Now instead of measuring the line-shape of I_f, i.e. the variation of

the intensity with the frequency of the fluorescence, we scan the laser frequency ν over the Doppler velocity range v/c of the particle speeds and measure the variation of the integrated intensity of the fluorescence.

iv. Figures 1 and 2 show typical data from an experiment of the type described in Section II [7]. Here a collisional plasma subject to crossed E and B fields is seen to support ion distribution functions whose shift and widths are both directly dependent on the fields and the collisionality. The technique used is "flash" LIF, with a short pulse (10 nsec) of resonant radiation from a tunable laser exciting transitions from long-lived "ground" states of NeII or ArII, to short-lived excited states. The laser beam intersects the light-collecting lens system at right angles, defining a viewed volume of about 3 mm extent in each spatial direction. Both the time and space resolution are small in comparison with plasma parameters, which are a few μsec for the time evolution, and a fraction of a centimeter for the gradient, respectively. The timing of the laser pulse and the viewed volume can both be scanned independently across the plasma. The velocity resolution is governed by the width of the laser line, typically 1 GHz in the visible or roughly 0.05 eV in ArII. Since the experiment is concerned with temperature rises up to several tens of eV, the resolution is evidently sufficient to provide the answers to the original problem. Note the distortions from the Maxwellian line-shape which occur at high electric fields. One can estimate these to be of order 1 eV, but the velocity resolution used here is clearly insufficient to quantify such results. In addition, at these high ion temperatures the Larmor orbits become comparable to the spatial resolution. For instance, with NeII at 16 eV and 3 kG, typical in this experiment, the Larmor radius is twice the spatial resolution and comparable to the mean gradient. I.e. there is coupling and overlap between elements of phase space. This demonstrates that, even though enhanced resolution in both wavelength and space is needed and can in principle be obtained, non-local effects introduce ambiguity and ultimately require a more sophisticated diagnostic altogether. This is discussed in the following section.

IV. IRREVERSIBLE PROCESSES: CAUSALITY AND TRANSPORT

Closer analysis reveals that LIF as described above, while fulfilling the needs of the description, falls short in one respect at least: it does not reveal enough about the discrete-particle nature of the plasma. This is best seen by applying the particle-exchange criterion. If two ions with different spatial positions but the same velocity were transposed, LIF would still yield the same signal. Optical Tagging (OT) was developed to overcome this limitations. It adds to phase space the dimension of memory, by telling us not only how many particles with a given velocity are found at a point, but also how and when they got there [8].

Tagging operates by remotely creating or destroying sets of particles into a specific quantum state - the test-state - in a given volume of phase space designated the "source". LIF is then used to isolate and follow the evolution of the test state in the space, time and velocity coordinates away from the source. OT requires at least a 3-level system possessing one long-lived quantum state. Figure 3 shows such a scheme, similar to a 2-state system but with the essential addition of a transition with strong branching from E to the metastable state M, which does not return to the ground-state, or else is long-lived enough so the decay to the ground-state occurs outside the field of analysis.

In OT, a pump laser P beamed across the source volume is tuned to the transition G-E. A fraction of the E-state particles created will decay to M, pumping up the metastable state density and depleting the ground-state. Both the "hole" in the G-density and the excess in M density diffuse away under the influence of conventional plasma processes, convecting quantum-state changes from the source. These changes are picked up by a second, search (S) laser-tuned to a transition characteristic of the test-state. Space-time correlation between P and S-lasers and the signals (fluorescence) they elicit serves to describe the transport of particles in the plasma.

A. Basic Model

The full range of possibilities of OT makes use of narrow-band tunable P and S lasers. Each laser selects out, at its coordinate position, a restricted velocity group of ions. Therefore, resonance of ions with both lasers implies a specific correlation between ion positions and velocities, enabling the phase-space trajectory to be traced out directly. The resolution is governed by the laser spectral widths, beam diameters and divergence, and the use of crossed-lasers to define points in space. This concept is illustrated and experimentally tested by following the space-velocity history of ions in a simple geometry where a closed-form calculation is possible: a uniform magnetized plasma column. In the absence of an electric field, and neglecting collisions, the equation of motion involves the Lorentz force only :

$$\frac{d}{dt}V = \frac{e}{m}\left(\frac{V \times B}{c}\right) \tag{14}$$

Let B define the z axis. Then the well-known axisymmetric solutions of Eq. (14) are :

$$v_x(t) = V \sin\phi \qquad v_y = V \cos\phi \qquad v_z = v_z \text{ , a constant} \tag{15}$$

That is, ions move with a constant speed v_z along the magnetic field, while their transverse velocities undergo harmonic motion with magnitude V and phase $\phi \equiv eBt/mc + \phi_o$. Here V and ϕ_o are constants determined by the initial conditions $v_x(0)$, $v_y(0)$ in accordance with:

$$v_x(0) = V \sin\phi_o \quad ; \quad V = \sqrt{v_x(0)^2 + v_y(0)^2}$$
$$v_y(0) = V \cos\phi_o \quad ; \quad v_x(0)/v_y(0) = \sin\phi_o/\cos\phi_o \tag{16}$$

We can transform the time to the space domain linearly, using the constancy of v_z. In moving from the plane z = 0 at time $t = t_o$ to

the plane z at time t, the ion displacement component along the z-axis is $z = t \cdot v_z$, and the phase ϕ increases from ϕ_o to $\phi = (\phi_o + z)$, where $\hat{z}$ is the normalized displacement $\hat{z} \equiv eBz/mcv_z$. Introducing this ϕ into Eq. (15), one obtains the space-dependent velocities :

$$\begin{aligned} v_x(z) &= V \sin(\phi_o + \hat{z}) \\ v_y(z) &= V \cos(\phi_o + \hat{z}) \\ \Rightarrow\ & V[\cos\phi_o \cos \hat{z} - \sin\phi_o \sin \hat{z}], \text{ by expanding the sum.} \end{aligned} \tag{17}$$

For simplicity, choose a geometry in which the P and S lasers are parallel to each other, defining the y axis, and spaced apart a distance z along this axis, at the same value of x. If they are both tuned to the same frequency, e.g. two beams derived from the laser, they resonate only with ions having the same value of v_y. Therefore, the condition for a group of ions to be pumped into the M-state at z = 0, and also to fluoresce on the M-E transition at z, is that they have the same value of the v_y component at both positions. Introducing this condition into Eq. (17) constrains the initial phases ϕ, in accordance with :

$$v_y(0) = v_y(\hat{z})$$

Now V is eliminated, and the condition yields :

$$\sin\phi_o/\cos\phi_o = (\cos \hat{z}-1)/\sin \hat{z} \tag{18}$$

Referring to Eq. (16), we see that this links the x and y velocities of the tagged ions. Note that the untagged ions should have, in this axi-symmetric configuration, independent x and y velocity components. One can express the velocity constraint in terms of a pseudo - temperature (as above for the collisional plasma), in the following way. Let the distribution function of transverse velocities for the ions be a Maxwellian :

$$f(v) \propto \exp - (v_{xo}^2 + v_{yo}^2)/T \tag{19}$$

Then the tagged ions are the sub-set with the distribution :

$$\begin{aligned} f_T &\propto \exp - v_{y0}^2 \left(1 + \frac{v_{x0}^2}{v_{y0}^2}\right)/T \\ &= \exp - 2v_{y0}^2/T(1+\cos \hat{z}) \end{aligned} \tag{20}$$

That is, the distribution function "seen" by the S laser, when scanned over frequency, appears to have an effective space-dependent temperature $T(1 + \cos \hat{z})/2$. Note that at $z = 0$, this coefficient of T starts out at 1; it reaches the minimum value 0 at $z = \pi v_z/2\omega_c$, and recovers its initial temperature one full cyclotron period later.

This dependence is precisely what is seen in the laboratory. Figure 4 shows two distribution functions, one at $z = 0$, the other at the minimum point, for ions tagged by two narrow-band lasers scanned in synchronism. The minimum "temperature" of 60° K represents the finite spectral width, divergence and positioning uncertainty of the two beams. Trace a shows the fluorescence of the background ions, corresponding to T = 2000° K. The tagged linewidth is so small that the hyperfine structure of the ion (BaII) emerges, even though the S laser is normal to the magnetic field. Figure c plots the spatial variation in the tagged-ion line width: the line represents the theoretical temperature variation $(1 + \cos \hat{z})/2$, which evidently fits the data.

B. Technical Aspects and Illustrations

Two operating modes are possible. Highest signal/noise is obtained in the "bright" mode, practicable with a system where the metastable-state population in the background plasma (i.e. without the P-laser) is small. An S-laser tuned to a frequency different from the P-laser is used, e.g. one tuned to the M-E transition. Because of the absence of M-states in the background, a diagnostic fluorescence excited by the S-laser can occur only where and when an M-state created at the source by the P-laser is present. Note that the S-laser, if narrow-band, defines a diagnosed volume in velocity as well as coordinate space. This provides a general method for correlating phase-space elements, including directivity, as demonstrated below. That is, it has the potential of yielding deeper information concerning the plasma state, e.g. correlations, than we will be concerned with here. A simpler version, the dark signal mode, uses as S-laser a beam split of the P-laser, i.e. tuned to the G-E transition. This searches out the hole in the depleted G-state, yielding decreased (negative) fluorescence since there are G-states present in the absence of the P-laser.

Inelastic collisions, which tend to destroy the identity of the test state, limit the spatial separation between source and diagnosed points for a single measurement to roughly one mean-free path. Figure 5 illustrates the measurement of diffusion along the magnetic field, by positioning the S-beam 2.5 cm axially "downstream" from the P-beam, and pulsing the P-intensity on with a 0.1 μsec rise-time, much shorter than the ion transit time τ between the two positions. Ions created in the M-state at P begin to arrive at S, which searches for (is tuned to) the M-E transition (bright mode), about 20 μsec after P switch-on, as shown by the delayed start of the S-beam induced fluorescence. As seen, I_f rises much more gradually (rise = 5 μsec), and decays much more slowly than the P-beam intensity. The peak in I_f, at 25 μsec, corresponds to a mean ion diffusion speed of 10^5 cm sec^{-1}. The rise- and fall-profiles in I represent the distribution of axial velocities, i.e. the ion parallel temperature, even though the P-laser beam is transverse to these velocities and cannot select them via the Doppler k•v term. This interpretation is checked out directly using LIF with a narrow beam parallel to the magnetic field.

An example of cross-field transport is shown in Fig. 6. Here ions are scattered by an electrostatic instability with strong cross-field electric components. Transport is measured by tagging ions at the center of the unstable plasma, and scanning the S-beam radially. Figure 6 plots the intensity I_f (density profile of diffused particles) as a function of radius, for increasing instability strengths. This traces particle transport extending to the plasma edge. Note that, because of radial weighting, the actual number of ions diffused to the edge appears less proportionally than it actually is. Here LIF in the S-beam provides not only density, but also temperature information on the diffused particles. This enables a complete physical description of the transport to be obtained. The insert in Fig. 6 plots the mean radius R_T, determined from the radially-weighted density profiles of the tagged particles. Also plotted is the mean Larmor radius increase R_L of these particles, calculated from their LIF Doppler widths. The correspondence of the two radii indicates that the nature of the diffusion is thermal. I.e. it represents the swelling of Larmor orbits due to ion heating by the unstable waves [8].

V. TIME, SPACE AND QUANTUM EFFECTS

As with all diagnostics, practicable schemes involve more than the simplest models (such as the 2-level system presented above) which serve to illustrate principles. As a result, the unfolding of LIF and OT data into physically significant information is a major concern in diagnostics. There are several fundamental causes for complexity in (A) the time, (B) coordinate and (C) velocity-space relationships between fluorescence signal and plasma properties, in multi-level atomic schemes. They apply to LIF as well as to OT diagnostics.

A. Time Dependences

It was shown above that a 2-level quantum system possesses an intrinsic time dependence, representing the finite evolution of the excited state population when the laser is switched on. In this simplest case it is an exponential with e-folding time which can be made short enough to be negligible in many classes of experiments. A much more complicated situation is obtained in 3-level systems [9]. An additional rate equation is involved, and the intrinsic time-dependence turns out to involve two exponentials, and becomes nonmonotonic. In fact the ground and excited states need not reach a finite-amplitude asymptotic level, instead they can become bleached or pumped out (depleted) by the laser beam - a drastic effect, since the diagnostic ends up unable to follow the plasma evolution. An example of slow intrinsic evolution is shown in Fig. 7. Here a laser is switched on, and the dependence of the fluorescence with time seen to change, even though the plasma remains constant. Note that the decrease, though monotonic, ends with the fluorescence at a finite value, i.e. the ground-state is not entirely depleted. The reason is that the ions here are flowing across the laser beam with a speed of the order of 10^5 cm sec^{-1}, convecting ground-state ions into the beam. The balance between such a source term and the laser-induced depletion maintains the finite level of diagnostic intensity.

A simple though inelegant way to avoid this type of distortion is to concede the game and resort to "flash" excitation, using a sequence

of laser pulses of short duration in comparison with the quantum lifetimes. Now each target state re-radiates only one photon into the viewed channel (the observed wavelength), so that $I_f \propto N_G(t_o)$. Equivalently, one turns on a long laser pulse, but enables (gates) the detection instrument during a short time only. This scheme obviously has lower signal/noise than continuously monitoring the fluorescence, as well as worse time resolution.

B. Spatial Resolution

Finite spatial dimensions also affect LIF. To illustrate this, consider the distortion induced in a 3-level system as a result of laser beam diameter (spatial resolution). This effect and its consequences on LIF diagnostics have been treated for a variety of models. In the steady state, target particles in the sub-class $N_G(v,x)$, move with velocity v along the x-direction across a continuous laser beam. To describe this condition, on the LHS of Eq. (9), one replaces $\delta/\delta t$ by $v(d/dx)$. Evidently in this mode each sub-population density evolves in space as it enters the laser beam. The spatial variable is $\tau = x/v$, thus the solutions are analogous to the time-dependent case with substitution of τ for t, hence sums of exponentials in τ. Because τ is dependent on v, particles with various v's have different density evolutions in x-space. As a consequence, depending on the geometry in which the observation is performed, different "mixes" of velocities are perceived. As an example, Fig. 8 shows the distorted distribution function obtained from a half-Gaussian flowing across a laser beam, where the parameter represents the ratio of the transit time (residence within the laser beam) to the upper-state lifetime. Distortion of this type are easily encountered, since the critical requirement is only that the transit time d/v of the particle across the beam diameter d be comparable to the atomic lifetimes, a condition easily met with hot ions ($v > 10^6$ cm sec^{-1}) and high-spatial resolution ($d < 1$ mm) laser beams, where $d/v < 10^{-7}$ sec, typically.

C. Power Broadening and Ground-State Lifetime

The existence of a suitable ground-state, its effective lifetime when including collisions and other inhomogeneous effects, are some of the central issues in LIF. One recalls that ionic first-excited states tend, because of the strong binding, to be at high energies above the ground-state, so that the transition frequency is beyond that available from commercial lasers, even with doubling. Consequently, the initial state in LIF schemes often is an excited, or at most metastable state, hence has a finite lifetime. Even when a true ground-state is used, collisions will cause it to have a finite lifetime T. Alternatively, transit across a finite-size laser beam, as above, may be viewed as imposing a finite lifetime on the ground-state.

These effects depend heavily, however, on the details of the quantum scheme involved. We illustrate this by considering an important process in LIF, power-broadening of the observed line profile, for two realistic systems: two-level, and three-level atoms. The technique used is that of the illustrations above, a very narrow-band tunable laser of intensity $I(\nu)$, whose center frequency ν is scanned across the Doppler profile of the particles. The ground-state population is now considered to consist of sub-groups $N_G(v)$ of velocity v: for any frequency, that sub-group is excited by the laser whose velocity satisfies the Doppler conditon $k\cdot v/kc = (\nu-\nu_f)/\nu_f$, within the uncertainty given by the linewidth, e.g. the frequency-dependence of the cross-section, such as the Lorentzian form, eq. 13 (in the limit of low intensity). That is, an intrinsic frequency dependence of the fluorescence intensity I_f exists, which tends to mask the v-dependence of the plasma ground-state distribution.

Consider to start with the elementary 2-level scheme without source terms, described in section III.C. In the steady-state, eq. (12) yields:

$$I_f = AN_E = g_G N_G \frac{A\sigma(\nu) I}{\Sigma g\sigma(\nu) I + A} \qquad (21)$$

Here the intrinsic frequency dependence is buried in the cross-section

$\sigma(\nu)$, appearing in the numerator and denominator. It is convenient instead to exhibit this ν-dependence explicitly. Substituting eq. (13) for σ, one obtains instead of eq. (21) the expression:

$$I_f = g_G A I \; N_G(v) L(\nu,\nu)/\Sigma g(I+I_1) \tag{22}$$

where the power-broadened line shape L is:

$$L = \frac{(A/2)^2 [1+I/I_1]}{[\nu - \nu_f(1-K\cdot V/KC)]^2 + (A/2)^2[1+I/I_1]} \tag{23}$$

and I_1 is the saturation parameter defined as:

$$I_1 \equiv A/\Sigma g\sigma_o \tag{24}$$

with σ_o the peak-value of the cross-section σ. Note that L is still Lorentzian, but that the full width at half amplitude has increased from the homogeneous value A by the intensity-dependent factor $(1 + I/I_1)^{1/2}$. As I increases, the uncertainty within which I_f localizes the velocity space location of $N_G(v)$ becomes larger.

To illustrate the importance of quantum effects, we now add a third level M to the scheme (as in Optical Tagging), as well as a source function (inhomogenous term) to represent processes such as collisions, particle flow, or other intensity-independent processes which enter the rate equations to create or destroy quantum states. For simplicity, the non-degenerate limit with g = 1 is taken, and a single time-constant T used to characterize all the source terms. Solving the rate equations in the steady state for this model [10], it turns out that the intrinsic ν-dependence of L has the same form as eq. (23), except that now the saturation parameter becomes:

$$I_1 = \frac{A_G + A_M}{2\sigma_0} \; \frac{1+1/\Sigma AT}{1+A_M T/2} \tag{25}$$

Here A_G, A_M are the two decay rates, from excited to ground and metastable states respectively. As can be seen, the two types of processes added have opposite effects. Branching reduces I_1 by the fac-

tor $(1 + A_M T/2)$, while source terms increase it by $(1 + (\Sigma AT)^{-1})$. Thus I_1 is quite model-sensitive. Note that, for some typical conditions, $A = 10^8$ sec^{-1} and $\sigma_o = 10^{-10}$ cm^2, so that in the visible (photons with energy ~3 eV) I_1 is a fraction of a Watt/cm^2, indicating that saturation and power-broadening occur at very low intensities. One sees also that T becomes important whenever inhomogenous processes have rates comparative to the decay rates.

The trade-off between laser intensity and velocity resolution is particularly important in configurations when a large - volume plasma is to be diagnosed with high spatial resolution. Here the laser diameter, and hence the volume of plasma excited by the laser, is made to be small, but the volume viewed by the detection optics lens is the entire double-cone subtended by the intersection of lens and laser axes [11]. Spontaneous emission or bremsstrahlung from this double-cone can reach the detector and constitutes a large noise term. This competes with the fluorescence induced by the laser, whose intensity I_f is linear in I at low intensities, but saturates as $I \gg I_1$ (see, for instance, eq. 22) as well as broadens. While the disadvantages of the intensity saturation are mitigated by the fact that, in this limit, variations in the laser power no longer affect the fluorescence, the broadening feature may obscure the essential physics of the problem.

It should be noted that the effects discussed in A. and B. above are interconnected with those of the quantum models presented here. This becomes evident when we consider, for instance, that one of the source processes which arises in a realistic geometry is the transit of particles across a finite-size laser beam. In the 3-level system above, this would be equivalent to replacing the time constant T by the transit-time d/v, whose effect was demonstrated in section A.

VI. CONCLUSIONS

The study of basic field-particle interactions has posed questions and challenges which have required and stimulated the development of new diagnostic methods based on atomic physics and laser techniques. As a result, the behaviour of ions (distribution functions and derived quantities: transport) can be measured with detail that would not have been imaginable in the past. The methods which have emerged are capable, by good chance, not only of answering the specific questions, but also of measuring additional properties of the plasma, and so are leading us on to suggest new experiments, where deeper levels of understanding can be tested. The electric and magnetic fields can also be inferred, but evidently the next steps in diagnostics will attempt more direct measurements: here one notes the ingenuity displayed by diagnosticians in the fusion area [12], and trusts that these will be refined further. As atomic and laser methods become more familiar, we are also led to appreciate the complexities involved, and begin to come up against intrinsic limitations and model dependences, as in all measurement methods. This requires attention to the field, but also pays off because the exciting and continual growth of these disciplines can provide new ways to interrogate the plasma.

ACKNOWLEDGMENTS

The hospitality and support of the California Institute of Technology and the Sherman Fairchild Foundation are gratefully acknowledged, as are the kind reception and active interaction afforded by the Applied Physics faculty and staff, especially Drs. P.M. Bellan, N.R. Corngold, R.W. Gould and P.C. Liewer of the Plasma Physics Group, and Drs. W.B. Bridges and A. Yariv.

FOOTNOTES AND REFERENCES

1. These lectures - not a review - put together selected case histories of experimentation in which the diagnostic component has been especially high, in the sense that the problem under investigation has called for the development of new measurement methods of general interest. It should be noted that fusion research has motivated a great variety of measurement schemes, which will be dealt with individually in lectures and workshop presentations at this School.

2. In gas discharges the field-particle interaction problem is particularly complex: in the simplest geometry, a potential difference is maintained across two electrodes, and the resulting plasma "seeks" a steady state in which the internal field distribution, and the densities, temperatures and velocities of the charged particles, are consistent with each other and the boundary conditions. This many-parameter problem should be contrasted with classical, and more tractable configurations, such as a steady-state plasma of known properties into which a small perturbation is injected. A recent conference report on gas discharge physics is "Electrical Breakdown and Discharges in Gases", ed. by E.E. Kunhardt and L.H. Luessen, Plenum, New York 1983.

3. The basic treatment is that of G.H. Wannier, summarized in his text "Statistical Physics", Wiley, New York 1966. Recent progress, including a discussion of the space dependence of the distribution function, can be found in J.E. Lawler, Phys. Rev. A32, 2977 (1985).

4. The use of laser-induced fluorescence for plasma diagnostics was first discussed conceptually by R.M. Measures, J. Appl. Phys. 39, 5232 (1968) and by D. Dimock, E. Hinnov and L.C. Johnson, Phys. Fluids 12, 1730 (1969). Initial experiments were carried out by C.F. Burrell and H.J. Kunze, Phys. Rev. Letters 28, 1 (1972); H.R. Döbele and K. Hirsch, Phys. Letters 54A, 267 (1975) on Helium and Hydrogen atoms in a plasma, respectively; and by R.A. Stern and J.A. Johnson III, Phys. Rev. Letters 34, 1548 (1975), and R.A. Stern, D.L. Correll, H. Bohmer and N. Rynn, ibid 37, 833 (1976) on ArII and BaII majority ions in a plasma.

Early reviews were presented by D.E. Evans and by H.W. Drawin in "Physics of Ionized Gases" ed. B. Navinsek, U. of Ljubljana, 1976. Other reviews can be found in P. Bogen and E. Hintz, Comments Plasma Phys. Cont. Fusion 4, 115 (1978); and G.T. Razdobarin and I.P. Polomkin, "Diagnostics for Fusion Experiments", Proc. of the Course, Varenna, 4-16 Sept. 1978, ed. by E. Sindoni and C. Wharton, Pergamon Press, 1979 and Sov. Phys. Tech. Phys. 24, 753 (1979). Some recent developments in this area are reviewed by R.A. Gottscho and Terry A. Miller, Pure and Appl. Chem. 56, 189 (1984), and R.A. Stern, Rev. Sci. Instrum. 56, 1006 (1985). High-resolution laser spectroscopy is recently reviewed in R.C. Johnson, Rep. Prog. Phys. 48, 531 (1985). Note that since the review by Razdobarin and Polomkin, no listing of the application of LIF to fusion research has adequately described the enormous progress achieved: this is, however, outside the bounds of our lectures.

5. H.J. Kimble and L. Mandel, Phys. Rev. A 13, 2123 (1976).

6. The interrelationship between particle velocity, electric and magnetic fields due to the Lorentz force, and their effect on atomic properties, is a major topic in itself. It promises to generate a new family of diagnostics: for instance, N.J. Wiegart, U. Rebhan and H.-J. Kunze, Physics Letters 90A, 190 (1982) propose the injection of a neutral Li beam into a magnetized plasma and LIF-measurement of the Stark line shift to deduce the value of the magnetic field component normal to the beam velocity. See also R.A. Stern, Rev. Sci. Instrum. 56, 1006 (1985).

7. F. Anderegg, R.A. Stern, F. Skiff, B.A. Hammel, M.Q. Tran, P.J. Paris and P. Kohler, Phys. Rev. Letters 57, 329 (1986): and unpublished material connected with the cited work.

8. R.A. Stern, D.N. Hill and N. Rynn, Physics Letters 93A, 127 (1983): R.A. Stern, Europhysics News 15, 2 (1984).

9. Early applications of multi-level scheme analysis to LIF diagnostics in plasmas are R.A. Stern, Phys. Fluids 21, 1287 (1978), and R.B. Wright, Nucl. Instr. and Meth. 170, 295 (1980). A typical experiment using 3-level systems is R.A. Stern, D.N. Hill and N. Rynn, Phys. Rev. Letters 47, 792 (1981).

10. P.G. Pappas, M.M. Burns, D.D. Hinshelwood, M.S. Feld and D.E. Murnick, Phys. Rev. A 21, 1955 (1980).

11. A.W. DeSilva and G.C. Goldenbaum, Meth. Exp. Physics, Vol. 9A (Academic, New York 1970), p. 111.

12. See, for instance, LIF diagnostics reported in the Proceedings of the 2nd International Symposium on Laser-Aided Plasma Diagnostics, Culham, September 1985.

FIGURES CAPTIONS

Fig. 1: Ion velocity distributions measured using Laser-Induced Fluorescence in rotating and heated plasma. Ordinate: fluorescence intensity. Abcissa: wavelength of laser radiation (linear scales). Center figure is measured at center of rotating plasma column, r = 0. Figures on either side are measured at r = ± 2 cm. on the same diameter (Reference 7, unpublished data).

Fig. 2: Diagram illustrating geometry and typical elements of an LIF experiment.

Fig. 3: Conceptual diagram of Optical Tagging Experiment. Top: trajectory of atom in quantum-state space; Bottom: trajectory in coordinate space.

Fig. 4: Distribution functions measured using Narrow-Band Optical Tagging. Traces a and b: ordinate, fluorescence intensity: abcissa, laser frequency (wavelength) (P and S ions at same position). Trace b shows tagged distribution, with S laser displaced by z = π. Trace c plots pseudo-temperature versus z. (Ref. 8).

Fig. 5: Ion Diffusion: Simultaneous measurements of ion diffusion and distribution function, using Broad-Band Optical Tagging. Ordinate, fluorescence intensity: abcissa, time (linear scales). (Ref. 8).

Fig. 6: Cross-field transport measurement of ions, using Narrow-Band Optical Tagging. Insert plots mean transport radius R_T and mean thermal (Larmor) radius R_L versus excitation voltage driving the plasma instability. (Ref. 8).

Fig. 7: Intrinsic time-dependence of signal in LIF. Stationary plasma (Ba II) is illuminated by pulse of resonant radiation of constant intensity, switched on at t = 0. Dashed curve shows theoretical response, using a 3-level model with inhomogenous (source) term representing flow of ground state ions across the laser beam (Ref. 9, Stern, Hill and Rynn, unpublished data).

Fig. 8: Distorted distribution functions in transit-time LIF configurations. Traces show calculated LIF velocity profile obtained from a half-Maxwellian streaming across the laser beam. Ordinate, relative number of particles (fluorescence intensity). Abcissa, velocity, normalized to thermal speed of half-Maxwellian. Curve parameter: ratio of transit time to characteristic excitation time (Ref. 9, Stern).

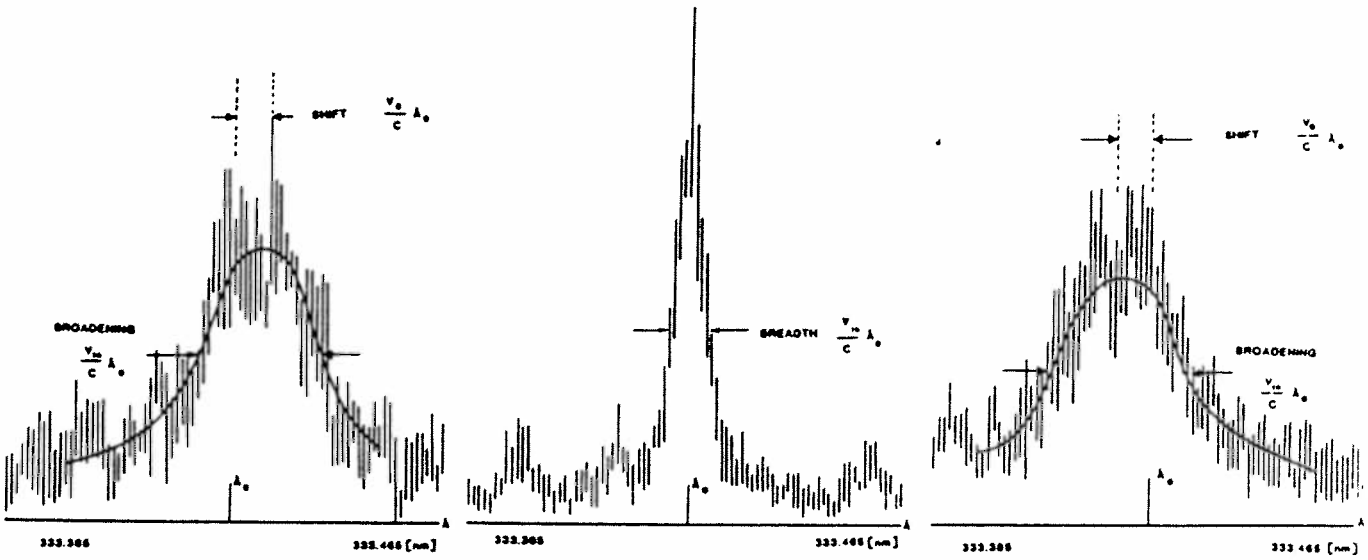

FIGURE 1

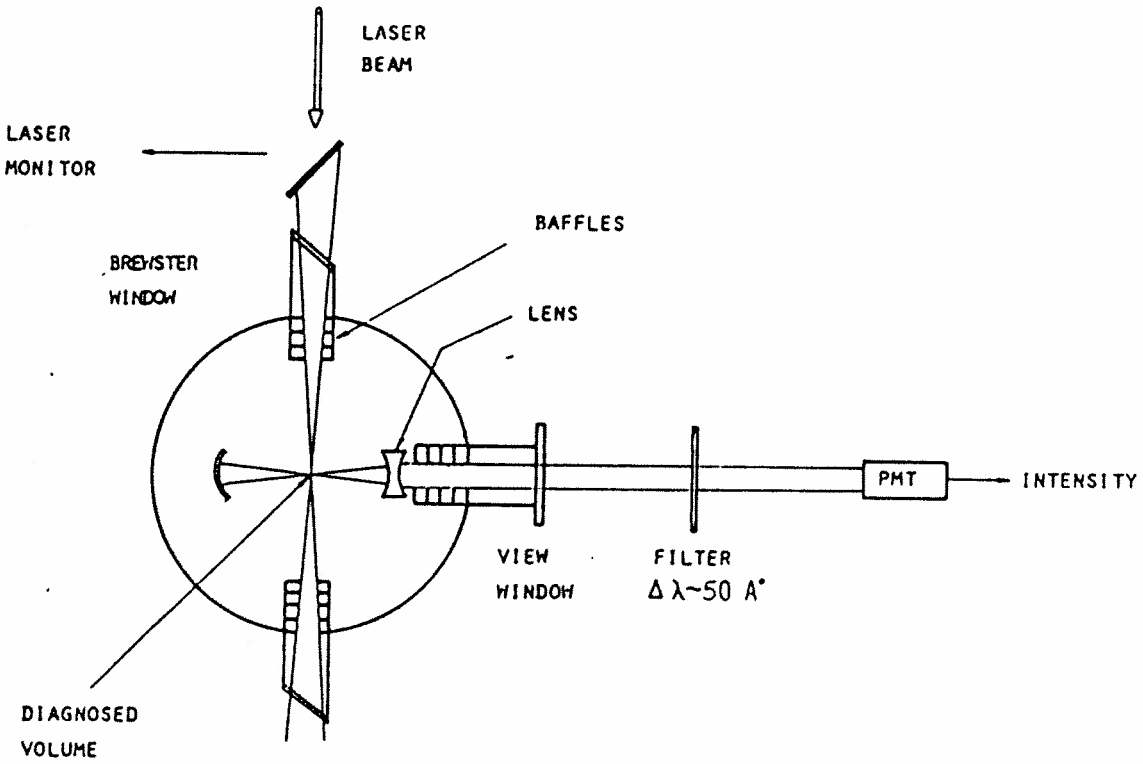

CROSS - SECTIONAL SCHEMATIC

FIGURE 2

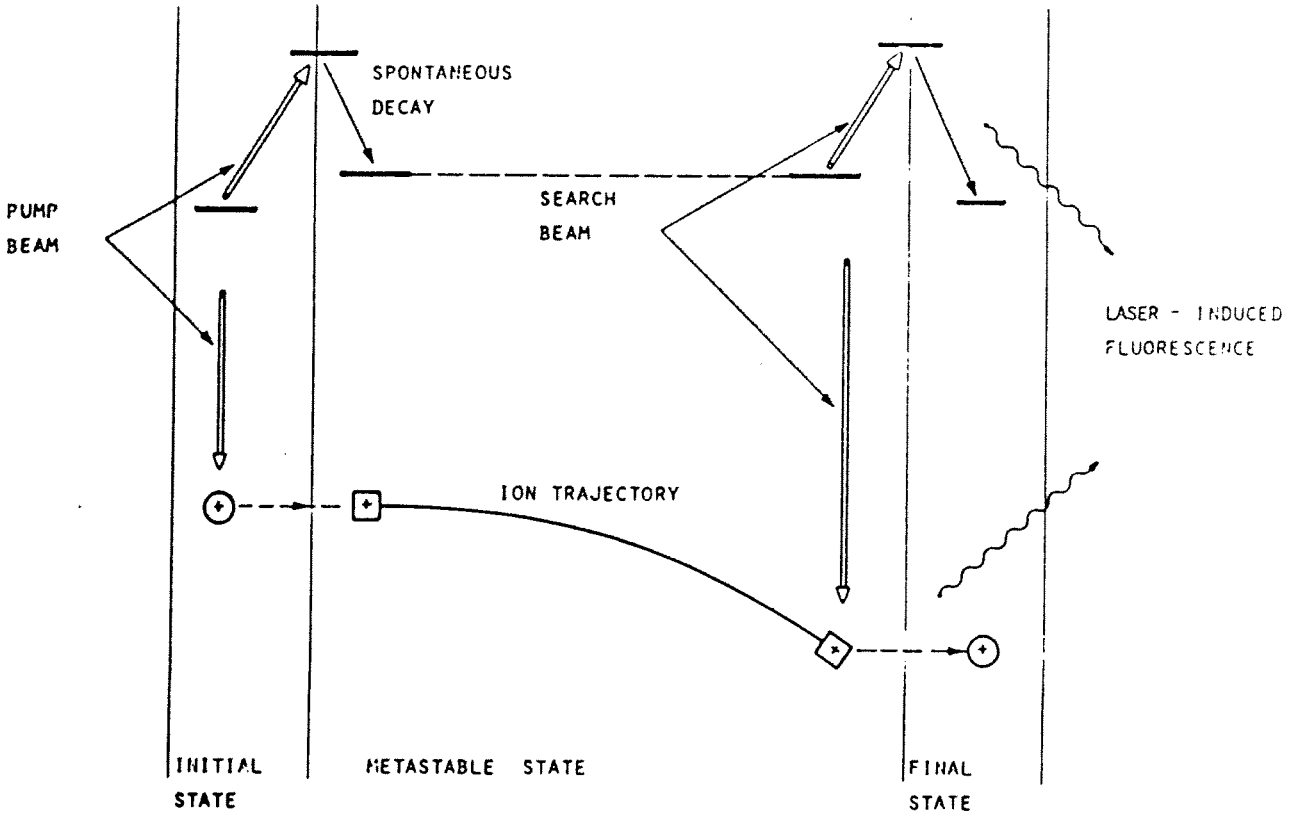

FIGURE 3

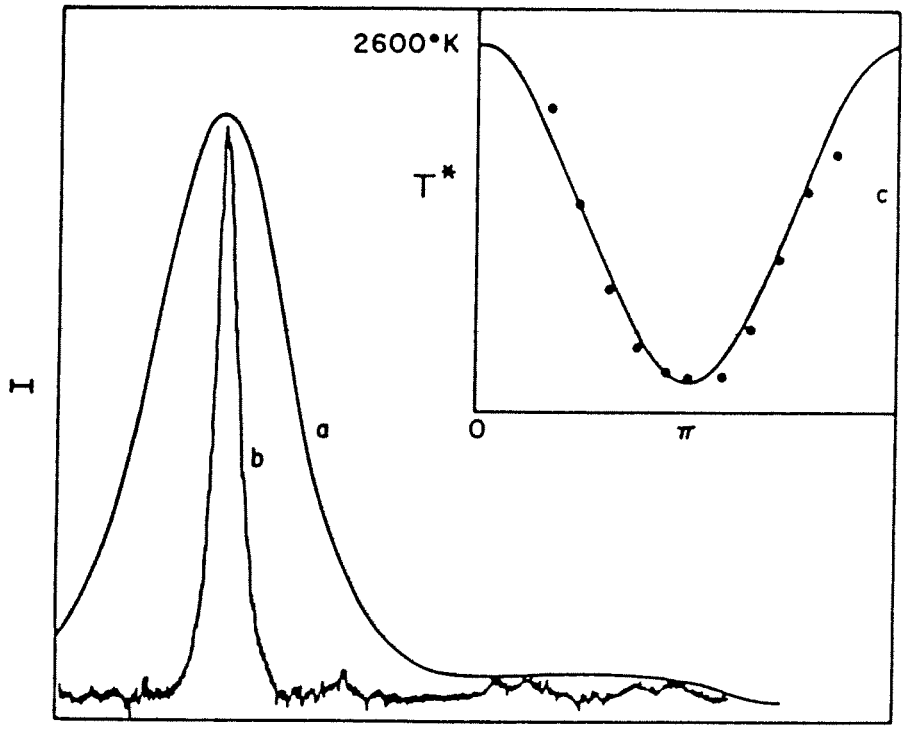

FIGURE 4

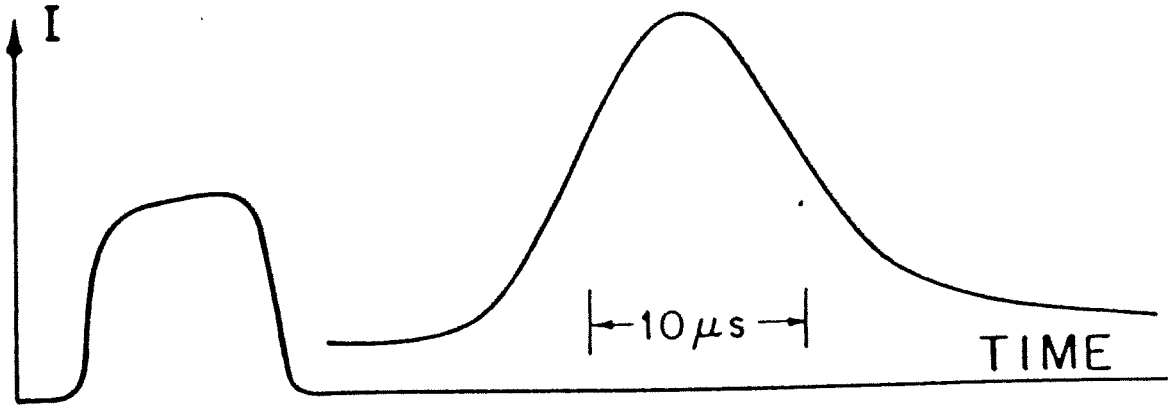

FIGURE 5

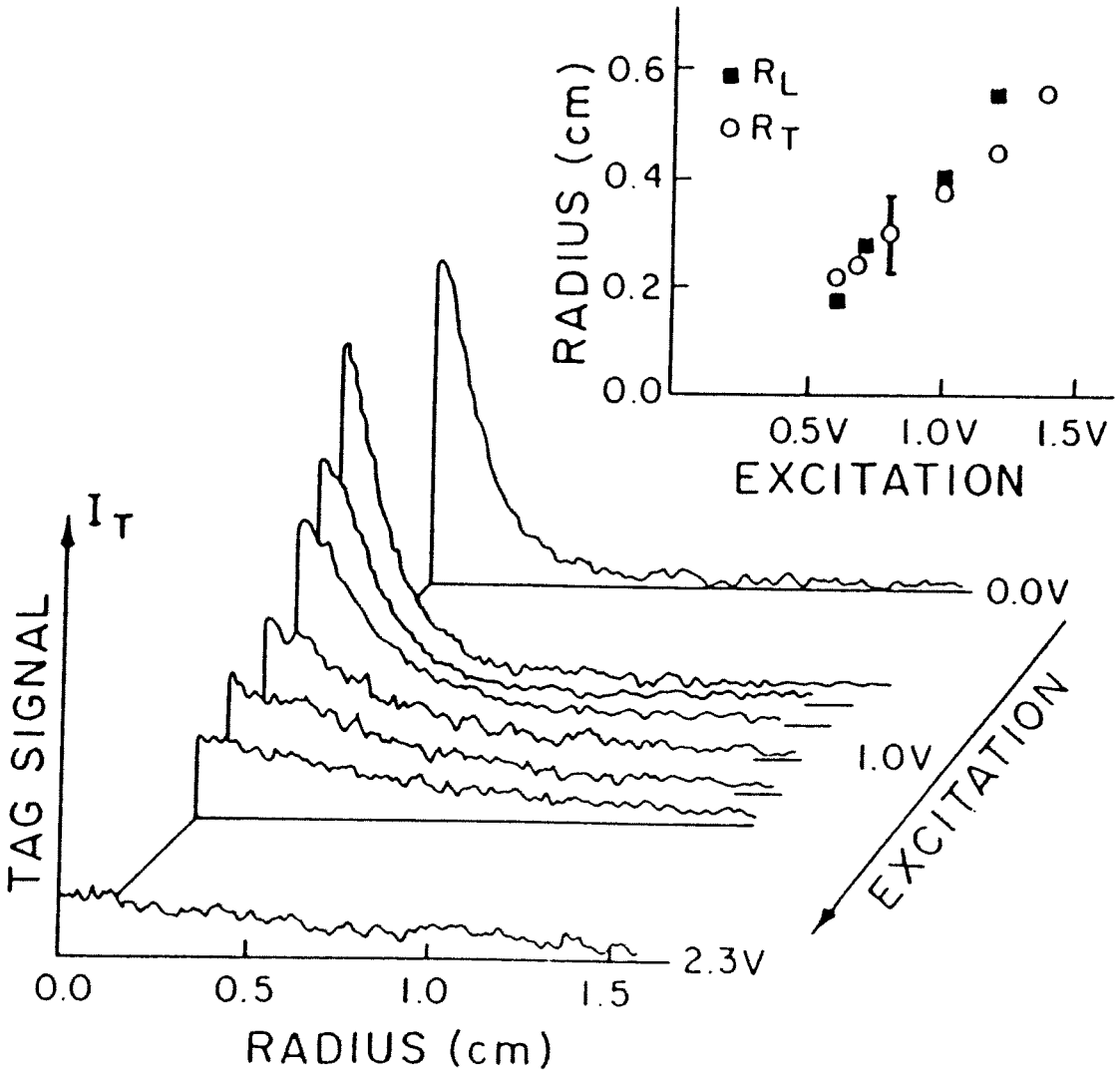

FIGURE 6

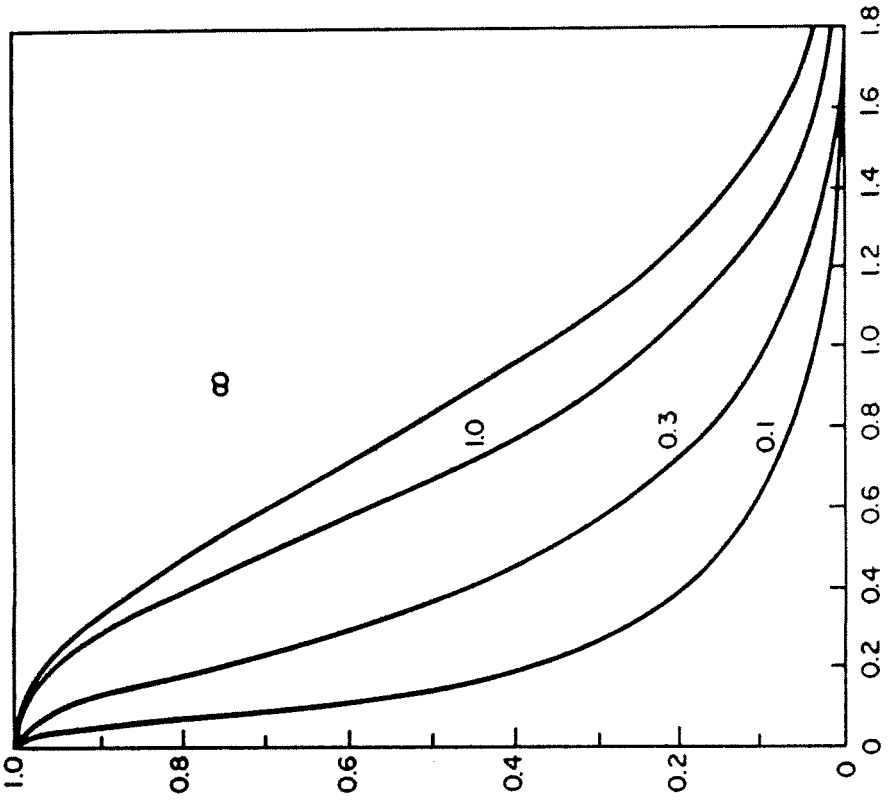

FIGURE 8

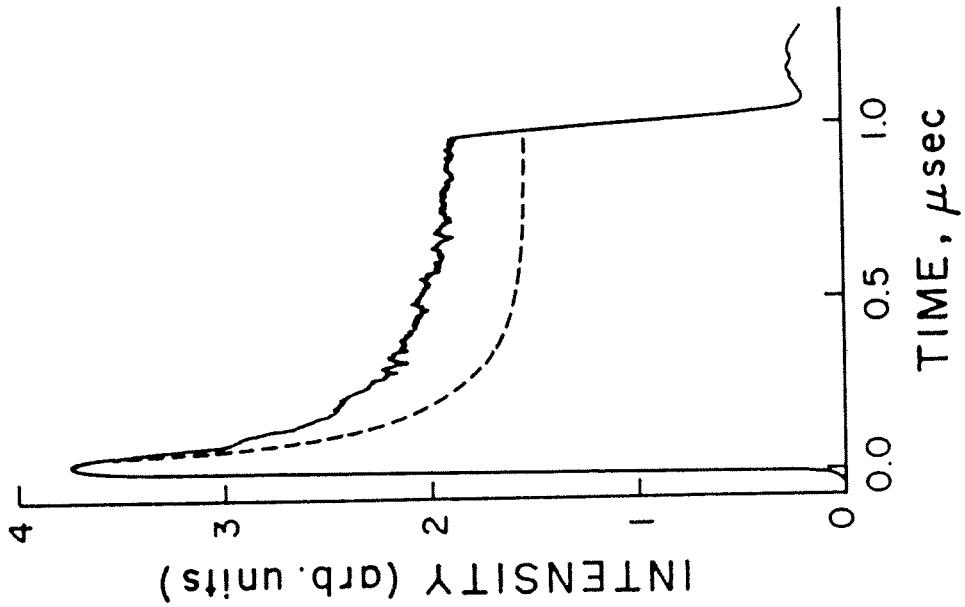

FIGURE 7